

# Collisional relaxation of Feshbach molecules and three-body recombination in $^{87}\text{Rb}$ Bose-Einstein condensates

G. Smirne,<sup>1</sup> R.M. Godun,<sup>1</sup> D. Cassettari,<sup>1</sup> V. Boyer,<sup>1</sup> C.J. Foot,<sup>1</sup> T. Volz,<sup>2</sup>  
N. Syassen,<sup>2</sup> S. Dürr,<sup>2</sup> G. Rempe,<sup>2</sup> M.D. Lee,<sup>1</sup> K. Góral,<sup>1</sup> and T. Köhler<sup>1</sup>

<sup>1</sup>Clarendon Laboratory, Department of Physics, University of Oxford, Parks Road, Oxford, OX1 3PU, UK

<sup>2</sup>Max-Planck-Institut für Quantenoptik, Hans-Kopfermann-Strasse 1, 85748 Garching, Germany

(Dated: March 23, 2022)

We predict the resonance enhanced magnetic field dependence of atom-dimer relaxation and three-body recombination rates in a  $^{87}\text{Rb}$  Bose-Einstein condensate (BEC) close to 1007 G. Our exact treatments of three-particle scattering explicitly include the dependence of the interactions on the atomic Zeeman levels. The Feshbach resonance distorts the entire diatomic energy spectrum causing interferences in both loss phenomena. Our two independent experiments confirm the predicted recombination loss over a range of rate constants that spans four orders of magnitude.

PACS numbers: 34.50.-s, 03.75.-b, 34.10.+x, 21.45.+v

Few-body collisions determine the lifetimes of cold gases of atoms and diatomic molecules. Recent experiments on identical Bose atoms [1, 2] suggest that magnetically tunable interactions [3, 4] in combination with such scattering phenomena could allow association of atomic clusters at rest [5] and confirmation of long standing predictions of quantum physics [6]. Destructive interferences of inelastic three-body collisions have paved the way for the Bose-Einstein condensation of  $^{133}\text{Cs}$  [2]. Scattering processes involving three atoms are known as three-body recombination and atom-dimer collisions. Three-body recombination refers to the threshold-less transition from initially unbound atoms to a dimer molecule and a remnant atom in accordance with energy and momentum conservation. All three atoms are lost from a cold gas. Previous theoretical studies relied upon model calculations [7] or analytic estimates [8], suggesting general trends for the behaviour of recombination rates in the limit of large diatomic scattering lengths. Several *ab initio* approaches to cold atom-dimer collisions [9] are presently limited to comparatively tightly bound diatomic states with energies up to about  $-k_B \times 1\text{ K}$  ( $k_B = 1.38 \times 10^{-23}\text{ J/K}$ ). The energies of dimers produced via magnetically tunable interactions are, however, typically on the order of  $-k_B \times 1\text{ mK}$ , right below the dissociation threshold.

In this paper we predict, for the first time, the atom-dimer collision rates involving such Feshbach molecules, consisting here of  $^{87}\text{Rb}$  atoms, without any adjustable parameters. Our exact approach to the three-body Schrödinger equation explicitly accounts for the coupling between the atomic Zeeman states. This allows us to properly describe the magnetic field dependent distortion of the diatomic bound state energies [10, 11] caused by the weakly coupled Feshbach resonance [12, 13]. We predict constructive and destructive interferences in both atom-dimer relaxation and three-body recombination rates which we interpret in terms of resonance phenomena associated with meta-stable trimer or bound dimer levels. Our approach has been tested by two independent experiments on three-body recombination in a  $^{87}\text{Rb}$  BEC over a range of rate constants that spans four orders of magnitude.

The three-body Hamiltonian,  $H_{3B}$ , is comprised of the ki-

netic energies of the atoms and their pairwise interactions, i.e.  $H_{3B} = H_0 + V_1 + V_2 + V_3$ . Here  $V_1$  is the potential associated with the interaction of the atom pair (2, 3), whereas  $V_2$  and  $V_3$  follow from cyclic permutations of the indices. We neglect short range genuinely three-body interactions as they are not expected to significantly affect resonance enhanced collisions. In the barycentric frame the total kinetic energy,  $H_0$ , can be divided into contributions from the relative motion of an atom pair and the motion of the third atom with respect to the centre of mass of the pair. Given the associated spatial Jacobi coordinates,  $\mathbf{r}$  and  $\boldsymbol{\rho}$ , respectively, such a separation yields:

$$H_0 = |\text{bg}\rangle \left( -\frac{3\hbar^2}{4m} \nabla_{\boldsymbol{\rho}}^2 - \frac{\hbar^2}{m} \nabla_{\mathbf{r}}^2 \right) \langle \text{bg}|. \quad (1)$$

Here  $m$  is the atomic mass and  $|\text{bg}\rangle$  indicates a product of ( $f = 1, m_f = 1$ ) Zeeman states [11] in which the three atoms of the  $^{87}\text{Rb}$  BEC are prepared. Depending on the context, we refer to either a product of three or two of such atomic ground states as the entrance-channel spin configuration and choose the zero of energy at its threshold for dissociation into unbound atoms.

To describe their initial and final configurations, we label each one of the colliding atoms by a Greek index  $\alpha = 1, 2, 3$ . The pairwise interactions,  $V_{\alpha}$ , determine the properties of cold diatomic collisions and highly excited molecular bound states, as well as their dependence on the magnetic field strength,  $B$ . In an idealised treatment, the observed resonant enhancement of the binary scattering length in the vicinity of  $B_0 = 1007.4\text{ G}$  [12, 13] arises from the near degeneracy of a single meta-stable diatomic energy level with the entrance-channel dissociation threshold. This bare Feshbach resonance level,  $|\phi_{\text{res}}\rangle$ , refers to a closed scattering channel comprised of Zeeman states from the excited  $f = 2$  level [11]. Accordingly, the interactions can be represented by [11]

$$V_{\alpha} = |\text{bg}\rangle V_{\alpha}^{\text{bg}} \langle \text{bg}| + W_{\alpha} |\phi_{\text{res}}\rangle_{\alpha} \langle \phi_{\text{res}}| + |\phi_{\text{res}}\rangle_{\alpha} \langle \phi_{\text{res}}| W_{\alpha} + |\phi_{\text{res}}\rangle_{\alpha} E_{\text{res}}(B)_{\alpha} \langle \phi_{\text{res}}|. \quad (2)$$

Here  $V_{\alpha}^{\text{bg}}$  and  $|\phi_{\text{res}}\rangle_{\alpha}$  are the diatomic entrance-channel potential and resonance level, respectively, whereas the third atom

with index  $\alpha$  is in the Zeeman ground state and plays the role of a spectator. Similarly,  $W_\alpha$  describes the pairwise inter-channel spin exchange coupling. The resonance state energy,  $E_{\text{res}}$ , depends on  $B$  through  $E_{\text{res}}(B) = \mu_{\text{res}}(B - B_{\text{res}})$ . Here  $\mu_{\text{res}} = h \times 4.2 \text{ MHz/G}$  is the difference in magnetic moments of closed- and entrance-channel atom pairs [10], and  $B_{\text{res}}$  indicates the point of degeneracy of  $E_{\text{res}}$  with the entrance-channel dissociation threshold. As the resonance state is weakly coupled, the shift  $B_0 - B_{\text{res}}$  is negligible [11]. Due to the absence of overlap between Zeeman states constituting the diatomic entrance ( $f = 1$ ) and closed ( $f = 2$ ) channels, all resonance states associated with different arrangements of the atoms are orthogonal:  $\langle \phi_{\text{res}} | \phi_{\text{res}} \rangle_\beta = \delta_{\alpha\beta}$ .

Our exact solutions of the three-body Schrödinger equation are based on the Alt, Grassberger, and Sandhas (AGS) technique [14]. Accordingly, we introduce the complete Green's function,  $G_{3B}(z) = (z - H_{3B})^{-1}$ , which characterises all bound and continuum levels of  $H_{3B}$ . Here  $z = E_i + i0$  is a complex variable indicating that the physical continuum energy of incoming particles,  $E_i$ , is approached from the upper half of the complex plane. Given the arrangement-channel and free Green's functions,  $G_\alpha(z) = (z - H_0 - V_\alpha)^{-1}$  and  $G_0(z) = (z - H_0)^{-1}$ , respectively, the AGS transition matrices,  $U_{\alpha\beta}(z)$ , are defined by implicit relations ( $\alpha, \beta = 1, 2, 3$ ):

$$G_{3B}(z) = \delta_{\alpha\beta} G_\beta(z) + G_\alpha(z) U_{\alpha\beta}(z) G_\beta(z). \quad (3)$$

In accordance with Ref. [14], these transition matrices determine, e.g., the Bose-symmetric scattering amplitudes for atom-dimer elastic or relaxation collisions by

$$f(\mathbf{q}_f, \mathbf{q}_i) = -\frac{8\pi^2 m \hbar}{9} \sum_{\alpha, \beta=1}^3 \alpha \langle \mathbf{q}_f, \phi_b^f | U_{\alpha\beta}(z) | \mathbf{q}_i, \phi_b^i \rangle_\beta. \quad (4)$$

Here  $|\mathbf{q}_i, \phi_b^i\rangle_\beta$  indicates an incoming dimer in the coupled-channels state  $|\phi_b^i\rangle$  of energy  $E_b^i$ , whereas the third atom with index  $\beta$  has the momentum  $\mathbf{q}_i$  with respect to the molecular centre of mass, and is described by  $\langle \rho | \mathbf{q}_i \rangle = \exp(i\mathbf{q}_i \cdot \rho / \hbar) / (2\pi\hbar)^{3/2}$ . Consequently, the initial state fulfils  $(H_0 + V_\beta) |\mathbf{q}_i, \phi_b^i\rangle_\beta = E_i |\mathbf{q}_i, \phi_b^i\rangle_\beta$  with  $E_i = 3q_i^2/(4m) + E_b^i$ . Similarly,  $|\mathbf{q}_f, \phi_b^f\rangle_\alpha$  describes the scattered atom and dimer, whose final energy,  $E_f = 3q_f^2/(4m) + E_b^f$ , equals  $E_i$ . The transition matrices in Eq. (4) are determined by the AGS equations [14]:

$$U_{\alpha\beta}(z) = (1 - \delta_{\alpha\beta}) G_0^{-1}(z) + \sum_{\gamma=1}^3 V_\gamma G_\gamma(z) U_{\gamma\beta}(z). \quad (5)$$

Based on Eq. (5), the upper panel of Fig. 1 illustrates the rate constants,  $K_{\text{ad}} = \sigma(q_f) q_f / (2m/3)$ , for elastic scattering ( $E_b^f = E_b^i = E_{-1}$ ) as well as relaxation ( $E_b^f < E_b^i = E_{-1}$ ) of  $^{87}\text{Rb}_2$  Feshbach molecules. Here  $\sigma(q_f)$  denotes the (in)elastic  $s$ -wave cross section associated with the amplitude of Eq. (4). Our implementation of Eq. (2) follows the approach of Ref. [15]. Consequently, the interactions properly describe: the measured  $B$ -dependences of the diatomic scattering length [13, 16], the binding energies of the two highest excited vibrational  $^{87}\text{Rb}_2$  states [10], their long-range wave

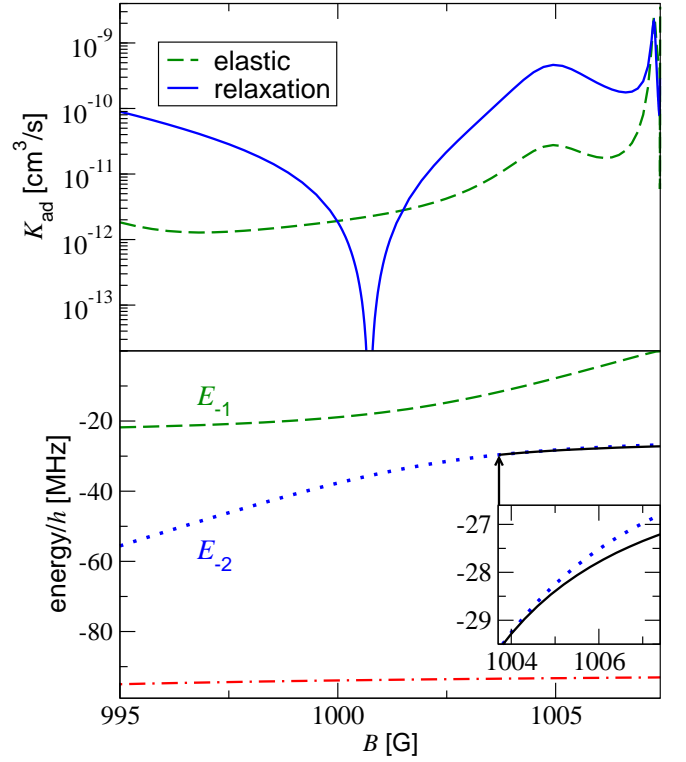


FIG. 1: (Colour online) Upper panel: Elastic (dashed curve) and inelastic (solid curve) atom-dimer scattering rates,  $K_{\text{ad}}$ , associated with a collision energy of  $3q_i^2/(4m) = k_B \times 10 \text{ nK}$  ( $k_B \times 1 \text{ mK} = h \times 20.8 \text{ MHz}$ ) versus  $B$  on the low-field side of  $B_0$ . Lower panel: Energies of the Feshbach molecular (dashed curve) and second highest excited vibrational (dotted curve) dimer states,  $E_{-1}$  and  $E_{-2}$ , respectively. The dot-dashed and solid curves indicate the energies of isotropic meta-stable  $^{87}\text{Rb}_3$  states. The highest excited trimer level emerges at about 1003.7 G (arrow) in a zero energy resonance (inset) for collisions between atoms and dimers in the second highest excited vibrational state.

functions as well as their entrance- and closed-channel spin admixtures [11]. The next vibrational dimer level is far detuned from the dissociation threshold by about 600 MHz [15] and will be neglected. Our predicted collisional relaxation rate constants are typically on the order of  $10^{-10} \text{ cm}^3/\text{s}$ . Such magnitudes have been confirmed by experiments on the stability of  $^{87}\text{Rb}_2$ , yielding  $K_{\text{ad}} = 2 \times 10^{-10} \text{ cm}^3/\text{s}$  at 1005.8 G [17] in good agreement with Fig. 1, as well as for  $^{23}\text{Na}_2$  Feshbach molecules [18]. Both species are associated with weakly coupled, closed-channel dominated [11], resonances. The fast atom-dimer decay tends to exceed elastic scattering, except for a region centred at about 1001 G, close to the avoided crossing of  $E_{-1}$  and  $E_{-2}$  at 1001.7 G [10] in the lower panel of Fig. 1. We expect relaxation into more tightly bound dimer states to partly fill in the gap in the inelastic rate constants.

Three-body recombination in a BEC is well described in terms of the transition from a continuum momentum state,  $|0, \text{bg}\rangle$ , associated with separated atoms at rest, to a dimer and a remnant atom. Whereas the initial state thus fulfils  $H_0|0, \text{bg}\rangle = 0$ , the final states are of the same nature as those

in atom-dimer relaxation and elastic collisions. In accordance with Ref. [14], the associated transition matrix is given by  $U_{\alpha,\beta=0}(z)$  of Eq. (3) with  $z = i0$ . For a definite target dimer state  $|\phi_b^f\rangle$  of energy  $E_b^f$  this matrix gives the loss rate constant to be:

$$K_3 = \frac{4\pi m q_f (2\pi\hbar)^6}{\hbar} \sum_{\alpha=1}^3 \int d\Omega |\alpha \langle \mathbf{q}_f, \phi_b^f | U_{\alpha 0}(i0) | 0, \text{bg} \rangle|^2. \quad (6)$$

Here  $d\Omega$  refers to the angular component of  $\mathbf{q}_f$  whose modulus,  $q_f$ , is determined by  $3q_f^2/(4m) + E_b^f = 0$ . The total loss rate constant,  $K_3^{\text{tot}}$ , is found by summation of Eq. (6) over all target states. Consequently, the number of condensate atoms,  $N$ , decays in accordance with

$$\dot{N} = -K_3^{\text{tot}} \langle n^2 \rangle N / 6. \quad (7)$$

Here  $\langle n^2 \rangle$  is the mean square density and the factor 1/6 accounts for the coherent nature of the gas [19]. The transition matrix,  $U_{\alpha 0}(i0)$ , can be inferred from the solutions of the AGS equations [14] using  $\beta = 0$  in Eq. (5).

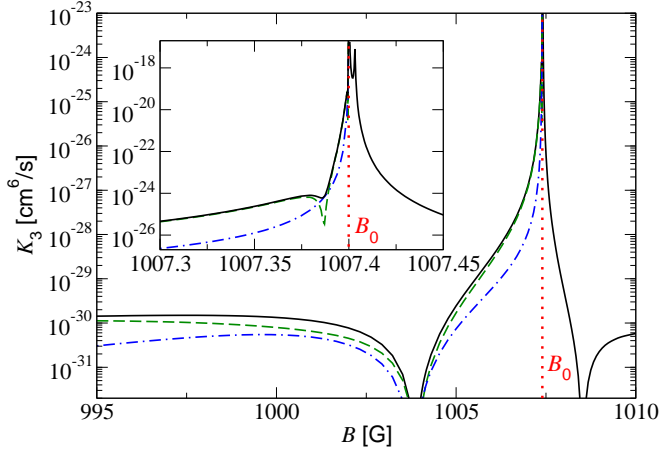


FIG. 2: (Colour online) Three-body recombination loss rate constant,  $K_3$ , versus  $B$ . Solid curves refer to the total loss rate constant,  $K_3^{\text{tot}}$ , whereas dashed and dot-dashed curves are its contributions from the final Feshbach molecular and second highest excited vibrational  $^{87}\text{Rb}_2$  states, respectively. The inset shows an enlargement close to the diatomic resonance whose position,  $B_0$ , is indicated by the dotted line.

Figure 2 gives an overview of the predicted total loss rate constants,  $K_3^{\text{tot}}$ , as well as their contributions from the different dimer target states. Recombination into Feshbach molecules dominates  $K_3^{\text{tot}}$  typically by an order of magnitude. Similarly to the atom-dimer collision rate constants of Fig. 1, the loss rate constant  $K_3^{\text{tot}}$  shows interference minima which may be attributed to  $B$ -dependent changes in the bound states of  $H_{3B}$ . Such isotropic trimer levels are indicated by the solid and dot-dashed curves in the lower panel of Fig. 1 and were determined using the Faddeev approach of Ref. [5]. The minimum of  $K_3^{\text{tot}}$  at about 1004 G in Fig. 2 occurs close to an atom-dimer zero energy resonance indicated by the arrow in Fig. 1. At the resonant magnetic field strength the trimer level becomes

degenerate with the second highest excited diatomic vibrational state where it can decay into a dimer and an atom in accordance with energy conservation. Both trimer levels of Fig. 1 are unstable with respect to such decay processes involving more tightly bound dimer states with energies below  $-\hbar \times 600$  MHz. In the inset of Fig. 2 the interference minimum below  $B_0$  and the maximum just above  $B_0$  can be attributed respectively to atom-dimer and three-body zero energy resonances associated with meta-stable Thomas-Efimov trimer levels [2, 5, 7]. Similarly, the oscillations in the atom-dimer collision rates close to  $B_0$  in Fig. 1 result from Efimov's effect [6], but their narrow magnetic field range makes this physics largely inaccessible to experiments on  $^{87}\text{Rb}$ . The minima of  $K_3^{\text{tot}}$  at about 1004 G and 1008.5 G in Fig. 2, however, could be resolved.

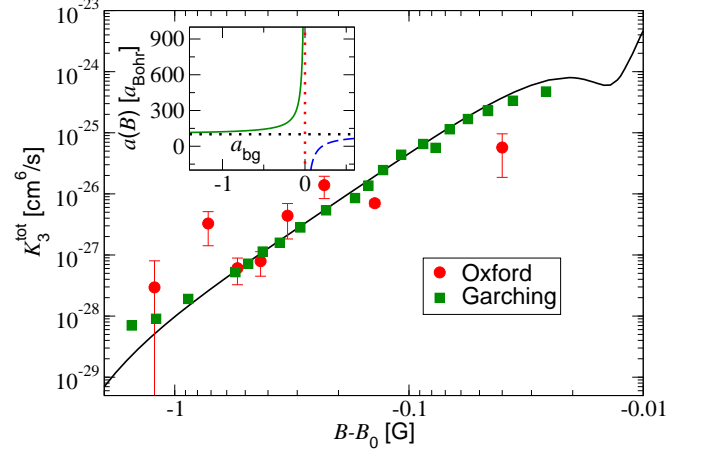


FIG. 3: (Colour online) Comparison between measured (circles and squares) and predicted (solid curve) total three-body recombination loss rate constants,  $K_3^{\text{tot}}$ . Error bars refer to statistical uncertainties only. The inset shows the binary scattering length,  $a(B) = a_{\text{bg}}[1 - \Delta B/(B - B_0)]$ , on the low-field (solid curve) and high-field (dashed curve) sides of the diatomic zero energy resonance (vertical dotted line). The horizontal dotted line indicates the background scattering length [13, 16]  $a_{\text{bg}} = 100.5 a_{\text{Bohr}}$  ( $a_{\text{Bohr}} = 0.0529$  nm) whereas the resonance width is  $\Delta B = 0.21$  G. All measurements refer to  $B < B_0$  where the BEC is stable with respect to collapse.

Figure 3 compares the predicted  $K_3^{\text{tot}}$  as a function of  $B$  with two independent experiments. In accordance with the inset, the measurements cover a range of diatomic scattering lengths from about 100 to 1000  $a_{\text{Bohr}}$  within which  $K_3^{\text{tot}}$  varies over four orders of magnitude. In the Oxford experiment, indicated by circles in Fig. 3,  $^{87}\text{Rb}$  atoms are loaded from a BEC into about 60 wells of a one dimensional optical lattice. The lattice is formed from a retro-reflected, vertical, 850 nm laser beam giving rise to individual wells with trapping frequencies (47, 47,  $1.75 \times 10^4$ ) Hz. The atoms are then prepared in the ( $f = 1, m_f = 1$ ) Zeeman ground state and a homogeneous magnetic field is ramped to a value  $B$  just below  $B_0$ . At this stage the atom number is  $N_0 = 3 \times 10^5$  and the mean square density is  $\langle n_0^2 \rangle = 2 \times 10^{28} \text{ cm}^{-6}$ . This is obtained by calculating the mean square density in each well using the BEC wave function from Ref. [20] and averaging

over the populated sites. After a hold time of  $\Delta t = 100$  ms, the magnetic field is ramped off and the final atom number  $N_f$  is measured. Assuming that coherence is maintained and that the volume of the cloud used to calculate the density  $n$  in Eq. (7) remains unchanged, the loss rate constant is extracted from  $K_3^{\text{tot}} = 6[(N_0/N_f)^2 - 1]/(2\langle n_0^2 \rangle \Delta t)$ . Uncertainties in  $N_0$  prevent measurements of  $K_3^{\text{tot}}$  below  $\sim 5 \times 10^{-28} \text{ cm}^6/\text{s}$ . We have confirmed this analysis by dynamical simulations of the experimental sequence using the non-linear Schrödinger equation with a three-body loss term.

In the Garching experiment, indicated by squares in Fig. 3, a BEC of  $5 \times 10^5$  atoms is loaded into a crossed-beam optical dipole trap [16]. After preparing the gas far away from  $B_0$  the magnetic field is ramped and held at its final value,  $B$ . For  $B < 1007.2$  G the size of the cloud changes adiabatically during the experimental sequence. Using the Thomas-Fermi prediction for the mean square density,  $K_3^{\text{tot}}$  is obtained from a fit of Eq. (7) to the loss data [21]. For  $B > 1007.2$  G the depletion is too fast for the BEC to adiabatically adapt its size. Consequently, we jump the magnetic field from the initial to its final value and measure the loss only on time scales sufficiently short for the cloud to keep its initial size. Systematic errors arise mainly from the calibration of the trap frequencies and the atom number, leading to an estimated uncertainty of a

factor of 3 in  $K_3^{\text{tot}}$ . Statistical errors are negligible in comparison. The accuracy of magnetic field calibration is 30 mG. We believe that our  $B$ -fields are sufficiently far from  $B_0$  for atom loss caused by collisional avalanches [22] to be negligible. As the BEC dynamics in the crossed-beam dipole trap is comparatively simple, the associated overall systematic uncertainty is smaller than in the optical lattice setup. The agreement within uncertainties between predicted and measured  $K_3^{\text{tot}}$  of both experiments in Fig. 3 confirms our approach.

We have shown how spin-dependent potentials can be included in a practical and exact treatment of three-body scattering phenomena. Destructive interferences predicted in atom-dimer relaxation rates allow elastic scattering of atoms from generally rather unstable  $^{87}\text{Rb}_2$  Feshbach molecules. The predicted magnetic field dependent suppressions of three-body recombination can be used to increase the lifetimes of cold gases [2]. While we have confirmed our approach by experiments on  $^{87}\text{Rb}$  condensates, it is applicable to all species, bosons and fermions, subject to closed- or entrance-channel dominated resonances [11].

This research has been supported by the Royal Society, the UK EPSRC, the EC Marie-Curie program, and the Cold Quantum Gases Network.

- 
- [1] C. Chin *et al.*, Phys. Rev. Lett. **94**, 123201 (2005).
  - [2] T. Kraemer *et al.*, Nature (London) **440**, 315 (2006).
  - [3] S. Inouye *et al.*, Nature (London) **392**, 151 (1998).
  - [4] J.L. Roberts *et al.*, Phys. Rev. Lett. **85**, 728 (2000).
  - [5] M. Stoll and T. Köhler, Phys. Rev. A **72**, 022714 (2005).
  - [6] V. Efimov, Phys. Lett. **33B**, 563 (1970).
  - [7] E. Nielsen and J.H. Macek, Phys. Rev. Lett. **83**, 1566 (1999); B.D. Esry, C.H. Greene, and J.P. Burke, *ibid* **83**, 1751 (1999); E. Braaten and H.W. Hammer, Phys. Rep. **428**, 259 (2006).
  - [8] D.S. Petrov, Phys. Rev. Lett. **93**, 143201 (2004).
  - [9] N. Balakrishnan, R.C. Forrey, and A. Dalgarno, Chem. Phys. Lett. **280**, 1 (1997); M.T. Cvitas *et al.*, Phys. Rev. Lett. **94**, 033201 (2005); *ibid* **94**, 200402 (2005).
  - [10] S. Dürr *et al.*, Phys. Rev. Lett. **92**, 020406 (2004).
  - [11] T. Köhler, K. Góral, and P.S. Julienne, Rev. Mod. Phys. **78**, 1311 (2006).
  - [12] A. Marte *et al.*, Phys. Rev. Lett. **89**, 283202 (2002).
  - [13] T. Volz *et al.*, Phys. Rev. A **68**, 010702(R) (2003).
  - [14] E.O. Alt, P. Grassberger, and W. Sandhas, Nucl. Phys. B **2**, 167 (1967).
  - [15] K. Góral *et al.*, J. Phys. B **37**, 3457 (2004).
  - [16] S. Dürr, T. Volz, and G. Rempe, Phys. Rev. A **70**, 031601(R) (2004).
  - [17] N. Syassen, T. Volz, S. Teichmann, S. Dürr, and G. Rempe, e-print cond-mat/0611047.
  - [18] T. Mukaiyama *et al.*, Phys. Rev. Lett. **92**, 180402 (2004).
  - [19] Yu. Kagan, B.V. Svistunov, and G.V. Shlyapnikov, JETP Lett. **42**, 209 (1985); E.A. Burt *et al.*, Phys. Rev. Lett. **79**, 337 (1997).
  - [20] P. Pedri *et al.*, Phys. Rev. Lett. **87**, 220401 (2001).
  - [21] J. Söding *et al.*, Appl. Phys. B **69**, 257 (1999).
  - [22] J. Schuster *et al.*, Phys. Rev. Lett. **87**, 170404 (2001).